9th International Food Operations & Processing Simulation Workshop
20th International Multidisciplinary Modeling & Simulation Multiconference

2724-0355 © 2023 The Authors.
doi: 10.46354/i3m.2023.foodops.001

# Numerical Analysis of Texture Modified 3D Printed Surimi gel: An opportunity to Produce Elder Friendly 3D Food

Timilehin Martins Oyinloye [1], and Won Byong Yoon[1 2, *]

[1]Department of Food Science and Biotechnology, College of Agricultural and Life Science, Kangwon National University, Chuncheon, Gangwon, 24341, Republic of Korea
[2]Elder-Friendly Food Research Center, Agriculture and Life Science Research Institute, Kangwon National University, Chuncheon, Gangwon, 24341, Republic of Korea

*Corresponding author. Email address: wbyoon@kangwon.ac.kr

## Abstract

With the growing population of elderly individuals and the increasing prevalence of dysphagia, the production of food that caters to their specific needs has become an urgent matter. One potential solution to address this challenge involves the utilization of 3D printing technology to create food with customized properties. The food industry has already harnessed 3D printing technology to generate unique textures and shapes that were previously unattainable using traditional food manufacturing methods. Surimi gel, a protein-based food material, serves as an exemplary instance of a food product that can be produced through 3D printing. However, the mechanical properties and texture characteristics of 3D printed surimi gels remain largely unexplored. In this study, our focus was on examining the modifications in texture achieved through 3D printing of surimi gel, aiming to create food that is suitable for elderly individuals and those with dysphagia. By employing numerical analysis, we evaluated the distribution of stress and strain during penetrative tests, and subsequently compared these findings with experimental data. Furthermore, we analyzed the impact of different structural variations on the texture characteristics of 3D printed surimi gels.

**Keywords:** 3D printing, surimi paste, numerical model, texture

## 1. Introduction

Surimi is a stabilized fish myofibrillar protein obtained from mechanically deboned fish flesh, that has been washed with water and blended with cryoprotectants (Lanier, Carvajal et al. 2005). It serves as the primary component in various surimi seafood products, such as steamed or fried fish cakes, crab sticks, and fish sausage (Park and Yoon, 2015). Recently, the integration of surimi into 3D printing technology has emerged, with its texture playing a crucial role in determining its acceptance among a diverse range of individuals, particularly the elderly (Wang, Zhang et al., 2018).

The texture properties of 3D printed surimi seafood are primarily influenced by two key parameters: the elastic and/or viscoelastic properties of the fish myofibrillar protein gels (Park and Yoon, 2015). These properties are particularly important due to the structural changes that occur in the myofibrillar proteins during the steaming process, which is a subsequent step in the 3D printing of surimi. The

© 2023 The Authors. This article is an open access article distributed under the terms and conditions of the Creative Commons Attribution (CC BY-NC-ND) license (https://creativecommons.org/licenses/by-nc-nd/4.0/).

myofibrillar proteins, specifically myosin and actin, form the contractile structure of surimi fibers and play a significant role in the formation of heat-induced gels. Upon denaturation, these proteins expose highly reactive surfaces. Heating salted surimi pastes causes the unfolding of proteins, leading to the interaction of neighboring protein molecules through the exposed reactive surfaces, resulting in the formation of intermolecular bonds. Sufficient bonding leads to the creation of a three-dimensional network, forming a gel (Cao, Fan et al., 2018). However, as the gel forms, moisture is gradually lost, causing an increase in the elastic and viscoelastic properties of the gel. These properties significantly contribute to the texture properties of the gel when it is used for 3D printing purposes.

Several mechanical tests have been employed to assess the texture properties of cooked or steamed surimi seafood, including compression or penetration tests using cylindrical, spherical, or conical probes, as well as extension (ring tensile) tests (Medina and Garrote, 2002; Park and Yoon, 2015). While the tensile properties of surimi gel are closely associated with sensory outcomes, the penetration test remains widely utilized in the seafood industry due to its straightforward measurement process (Tabilo-Munizaga and Barbosa-Cánovas, 2004).

The penetration measurements of food gels can yield varying texture properties due to differences in gel structure and the surface area that comes into contact with the probe and sample during analysis. Furthermore, the penetration test provides comparable information to the tensile test for elastomeric materials (Park and Yoon, 2015). Therefore, a comprehensive understanding of penetration measurements is a crucial parameter in the development of 3D printed food intended for the elderly, as it enables critical interpretation of texture properties and describes properties that resemble sensory characteristics in the oral cavity. To achieve this, numerical simulation has been successfully employed in conjunction with various texture methods to analyze the textural and viscoelastic properties of foods (Hong, Uhm et al., 2014; Zhang, Chu et al., 2016).

The utilization of numerical simulation provides a robust and nondestructive research tool for analyzing mechanical properties, including stress and strain, of food gels (Hong, Uhm et al., 2014; Zhang, Chu et al., 2016). The application of numerical simulation in understanding the large deformation properties of various materials has been extensively discussed in numerous studies (Bhashyam, 2002). Nonlinear models within numerical simulation tools can effectively simulate and predict the responses of reinforced and pre-stressed material components, as each component exhibits its own unique stress-strain behavior.

Several studies have been conducted to evaluate the mechanical properties of surimi gel, aiming to understand the impact of different additives on its texture attributes (Hsu and Chiang, 2002; Tabilo-Munizaga and Barbosa-Cánovas, 2004; Duangmal and Taluengphol, 2010; Park and Yoon, 2015). However, most of these methods involve destructive testing. Moreover, to fully comprehend and select the most suitable design for elder consumption, it is essential to investigate the effect of model structure and design on the penetration test of 3D printed surimi gel.

Hence, the objective of this study was to analyze the stress and strain properties of steamed 3D printed surimi gel during the cylindrical penetration test. The deformation characteristics of the steamed gel, with varying structures and designs, were also evaluated using numerical analysis methods. Additionally, the optimal volume fraction and model structure for developing elder-friendly 3D printed surimi gel were determined and confirmed.

## 2. Materials and Methods

### 2.1. Surimi gel preparation

In this study, a high quality (FA grade) Alaska pollock surimi with a 75% moisture content, 24.1% protein, 0.9% fat, and pH of 6.8 provided by Pulmuone Co., Ltd. (Gwangpyeong-ro, Seoul, South Korea) was used. The frozen surimi was thawed at room temperature (25 ± 2 °C) for 4 hr. The surimi block was chopped at 5 °C with a vacuum cutter equipped with a temperature control system (Model UMC5, Stephan Machinery Corp., Hameln, Germany). Based on our previous research on surimi 3D printing (Oyinloye and Yoon, 2022), the moisture content was adjusted to 82% during mixing. The 3D printing process was carried out on the surimi paste using optimized printing conditions: a volume flow rate of 2.5 × 10-8 m3/s, nozzle diameter of 1.0 mm, nozzle movement speed of 15 mm/s, and a layer height of 1.0 (Oyinloye and Yoon, 2022). A cube-shaped model with a length of 20 mm was designed and printed. The 3D printed gel sample was prepared by steaming the printed surimi paste on a perforated tray positioned at the center of a water bath system (Model BS-11, Jero Tech., Geomuldae-ri, South Korea). The steaming temperature was maintained at 90 °C for a duration of 30 minutes. Sample was not allowed to come into direct contact with the water. At the end of the steaming operation, sample was immediately cool to room temperature under running water. Analysis was conducted on the gel sample after 12 hours.

### 2.2. Critical model height determination

In this study, the determination of the critical height for developing the geometry of the 3D printed surimi gel was conducted by altering the number of stacked layers within the model, resulting in the omission of specific layers at certain positions (Figure 1). Due to the nature of the surimi paste, the previously printed

layers can only provide limited support for the layer height above the empty space. If the paste's height exceeds this limit, it will collapse before reaching the post-processing stage, which involves steaming. To identify the critical model height, the number of omitted layers was varied, specifically using 2, 3, and 4 layers, in order to create less dense models with hole sizes of 2 mm, 3 mm, and 4 mm in thickness, respectively. By experimenting with different configurations, the critical height necessary for maintaining structural integrity during the printing process and subsequent steaming was determined.

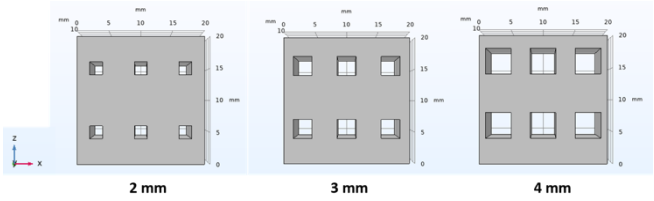


**Figure 1.** Schematic representation of model geometry for determining critical layer height.

## 2.3. Geometry model development and gel formation

Once the critical height was determined, further adjustments were made to the structural model by varying the volume fraction within the cubes. This adjustment was made specifically for models with a hole size less than or equal to the critical height. As illustrated in Figure 2, the models MD 1, MD 2, MD 3, and MD 4 represented full cube structures with varying volume fractions of 100%, 85%, 80%, and 75%, respectively. The sample was gently moved into the steam chamber (Model BS-11, Jero Tech., Geomuldae-ri, South Korea) immediately after printing was completed, and the steaming operation was conducted at 90 °C for 30 min. Subsequently, the steamed gels, with final moisture contents of 78.28 ± 0.57%, 75.91 ± 0.36%, 73.12 ± 0.43%, and 70.01 ± 0.33% for models MD 1, MD 2, MD 3, and MD 4, respectively, were placed in a plastic bag and rapidly chilled in ice water at 0 °C. After a 12-hour period, the texture properties of the cooled gels were evaluated.

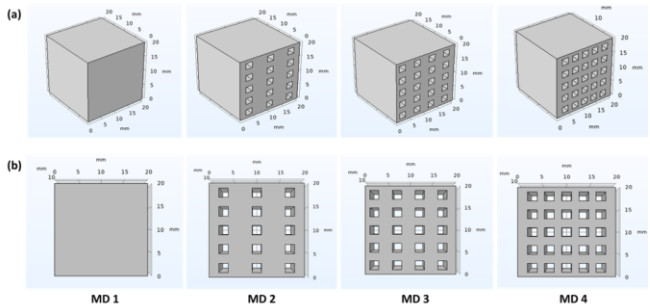


**Figure 2.** Schematic representation of model geometry for determining critical layer height.

## 2.4. Mechanical analysis of surimi gel

### 2.4.1. Texture property of 3D printed surimi gel

The penetration test was performed using a TA-XT texture analyzer (Stable Micro Systems, Surrey, UK) equipped with a cylindrical probe (Model: TA-54 with diameter 12.6 mm and height 35 mm). The penetration analysis conditions were set as a test speed of 0.5 mm/s and a travel distance of 15 mm down into the gel such that approximately 75% of the total gel height is punctured by the large deformation. The instantaneous penetration force (N), indicating the force measured for every distance traveled through the gel sample was measured. All measurements were conducted 10 times.

### 2.4.2. Mechanical properties of surimi gel

The mechanical properties of surimi gel were determined using the method described by Park & Yoon (2015). A compression test was performed on the 3D printed surimi gel (MD 1). The force-displacement data from the compression test was used to calculate the engineering stresses and strains using equations (1) and (2),

$$\sigma_{eng} = \frac{F}{A_0} \quad (1)$$

$$\varepsilon_{eng} = \frac{H_0 - H}{H_0} = \frac{\Delta H}{H_0} \quad (2)$$

where $\sigma_{eng}$ and $\varepsilon_{eng}$ are respectively the engineering stress and strain; F is the load (N) measured during the compression testing; $A_0$ is the initial cross-sectional area of the specimen; $H_0$ is the initial sample height, and H is the instantaneous height of the sample during compression. In engineering practice, the mechanical properties of materials are usually described by engineering stress-strain curves. However, in numerical simulation, material properties are commonly described with true stress-strain curves (Song and Sanborn 2018). In the uniaxial tension test, the true stress ($\sigma_{true}$) and true strain ($\varepsilon_{true}$) are calculated using equations (3) and (4), respectively.

$$\sigma_{true} = \sigma_{eng}\,(1 - \varepsilon_{eng}) \quad (3)$$

$$\varepsilon_{true} = -\ln(1 - \varepsilon_{eng}) \quad (4)$$

Information from true stress ($\sigma_{true}$) vs strain ($\varepsilon_{true}$) was used to determine Young's modulus ($E$) which is represented as the slope of the linear region before the yield stress point. For the numerical analysis, the region of plastic deformation in the stress-strain curve was used to analyze the elastic ($\varepsilon_{elastic}$) and plastic ($\varepsilon_{plastic}$) strain using equations (5) and (6), respectively,

$$\varepsilon_{elastic} = \frac{\sigma_{true}}{E} \quad (5)$$

$$\varepsilon_{plastic} = \varepsilon_{Total} - \varepsilon_{elastic} \quad (6)$$

where $\varepsilon_{Total}$ is the total strain.

## 2.5. Numerical analysis

Ansys 2020 R2 with Explicit dynamic module (Ansys, Inc., Canonsburg, PA, USA) was used to characterize the penetration effect on the surimi gel (i.e., using a cylindrical puncture).

### 2.5.1. Geometry description

The design of the sample geometry was modeled using ANSYS Workbench 2020 R2. The dimensions of both the surimi gel and probes matched those specified for models MD 1, MD 2, MD 3, and MD 4 for mechanical analysis (Figure 3). In order to create a mesh with elements of the same size as the layer height employed in 3D printing, a body sizing function was utilized. Additionally, a level 3 mesh refinement was implemented on the probe's wall to accurately capture the fracture properties in the sample model (Figure 3). A total of 12,617 to 14,281 elements were generated for the penetration test.

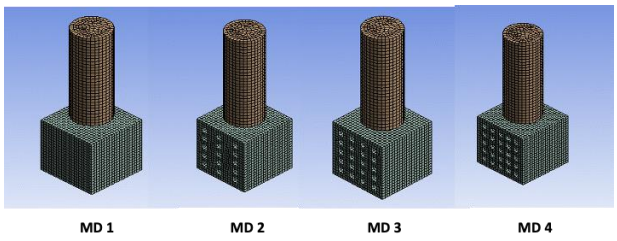


**Figure 3.** Geometry description of 3D printed surimi gel during numerical analysis for MD 1, MD 2, MD 3, and MD 4.

### 2.5.2. Finite element method (FEM) simulation for penetration process

The Johnson-Cook model dependent on temperature and strain rate was used for the FEM simulation (Krasauskas, Kilikevičius et al. 2014). In this case, the true stress is described by equation (7);

$$\sigma_{true} = \left(A + B(\varepsilon_{plastic})^n\right)\left[1 + C\ln\frac{\dot{\varepsilon}_{plastic}}{\varepsilon_0}\right]\left(1 - \left(\frac{T - T_{material}}{T_{melt} - T_{material}}\right)^m\right) \quad (7)$$

where $\sigma_{true}$ is the true stress, A is the initial yield strength of the surimi gel at room temperature, B is the hardening modulus, $\varepsilon_{plastic}$ is the true plastic strain, n is the strain hardening exponent, C is the parameter representing the strain rate sensitivity, $\dot{\varepsilon}_{plastic}$ is the true plastic strain rate, $\varepsilon_0$ is the reference strain rate, m is the parameter evaluating the thermal softening effect, T is the temperature, $T_{melt}$ is the melting point temperature, and $T_{material}$ is the material transition temperature. Since the influence of the temperature change due to the friction of the probe against the gel sample was not considered, the general form of the model in equation (7) becomes equation (8).

$$\sigma = \left(A + B(\varepsilon_{plastic})^n\right)\left[1 + C\ln\frac{\dot{\varepsilon}_{plastic}}{\varepsilon_0}\right] \quad (8)$$

A failure criterion is required to characterize the gel material properties degradation due to the probe penetration. The Johnson-Cook failure model based on plastic strain was used. In this model, the failure occurs when parameter D becomes 1:

$$D = \int \frac{1}{\varepsilon_f} d\varepsilon_{plastic} \quad (9)$$

where $\varepsilon_f$ is the true fracture strain. The true fracture strain is given by equation (10)

$$\varepsilon_f = \left(d_1 + d_2 exp^{-d_3\frac{\sigma_m}{\sigma}}\right)\left[1 + d_4 ln\frac{\dot{\varepsilon}_{plastic}}{\varepsilon_0}\right](1 + d_5) \quad (10)$$

where $d_1$ to $d_5$ are the material damage model constants obtained by the MATLAB curve fitting tool as $d_1 = 0.35$, $d_2 = d_3 = d_5 = 0.001$, $d_4 = 0.021$, and $\sigma_m$ is the mean stress.

The boundary conditions were set as follows; the bottom of the cube shaped gel was fixed, and the top of the puncture probe was assigned a total displacement of 15 mm, which translate along the negative z-axis at a displacement rate of 0.5 mm/s, and a frictional contact was established between the wall of the probe and the surface of the 3D printed gel.

One of the main challenges encountered during the simulation was excessive mesh distortion and failure in the convergence criteria, therefore an explicit finite element code based on the adaptive mesh technique was used, which allows the mesh to automatically regenerate when elements are distorted due to large deformations. In an explicit model, an adaptive mesh generates a new mesh and remaps the solution parameters from the old mesh to the newly generated one. In this study, adaptive meshing was performed for every three probe increments, with five mesh sweeps per adaptive mesh increment. Additionally, in order to shorten the computational time, the mass scaling technique was used which modifies the densities of materials in the model and improves the computational efficiency (Krasauskas, Kilikevičius et al. 2014). The mass scaling used in this study was performed every 10 increments to obtain a stable time gain of at least 0.0001 s step time.

## 2.6. Statistical analysis

We characterized at least five freshly prepared 3D printed gel samples for each analysis. Mean values and standard deviations were calculated for each measurement. Data were analyzed using the statistical analysis software SPSS 19.0 and results were reported as mean values ± standard deviations.

# 3. Results and Discussion

### 3.1. Critical missing layer height for 3D printed surimi

The critical layer height of the 3D printed surimi paste was determined through visual analysis. The size of the hole between the 3D printed model, as shown in Figure 4, directly impacts the structural stability of the paste. As the hole size increased from 2 to 4 mm, the previously printed layer became incapable of supporting the layers above the holes. Consequently, an intermediate layer experienced a significant collapse, particularly noticeable at the edges of the paste in the model with a 4 mm hole size. Conversely, the model with a 2 mm hole size demonstrated the ability to retain its shape and stability after printing. Hence, the 2 mm hole size was identified as the critical layer height for the less dense model, and subsequently, the number of holes was varied to create models MD 2, MD 3, and MD 4.

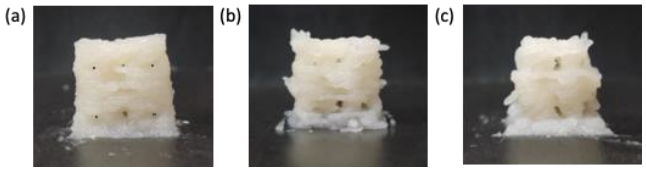


**Figure 4.** 3D printed surimi paste with different hole size for the determination of critical hole height; (a) 2 mm, (b) 3 mm, and (c) 4 mm.

### 3.2. Texture properties of 3D printed surimi gel

The texture properties of 3D printed surimi gel are presented in Figure 5. All force-displacement curves exhibit breakpoints, indicating the loss of gel structure integrity upon penetration by the cylindrical probe. The influence of the model structure was confirmed during the penetration test. Model MD 1 (100%) displayed a consistent increase in penetration force as the probe depth increased. In contrast, Models MD 2 (90%), MD 3 (80%), and MD 4 (70%) demonstrated a varying range of penetration forces with approximately three distinct levels. The initial increasing range was observed when the probe first punctured the gel sample. This puncture caused compression of the gel, enabling the filling of the holes created in the model by the gels in the upper layers. Consequently, as the number of holes increased, the rate of force increase at each level decreased. Thus, model MD 2 exhibited significantly greater penetration force compared to model MD 4. Moreover, when the entire hole was filled with the compressed sample, the detected force primarily comprised of normal and shear forces acting on the sample, resulting in similar peak forces across MD 2 to MD 4 (Figure 5).

Regarding the force required to puncture the gel samples, it was found that structure MD 2, MD 3, and MD 4 positively influenced a reduction of over 50% in the required force compared to the original model (MD 1). Consequently, the designed model can be effectively utilized in the development of food diets for the elderly or individuals with dysphagia, as it significantly reduces the force needed to chew the samples.

The adhesive properties of the 3D printed gel were observed for all models, and MD 1 exhibited a significantly higher value. Adhesiveness refers to the work required to overcome the adhesive force between the cylindrical probe (representing teeth) and the gel sample. High adhesiveness is associated with an increased risk of choking and requires more effort to propel the food bolus through the pharynx. Foods with high adhesiveness are not recommended for the elderly or individuals with swallowing difficulties (Suebsaen, Suksatit et al., 2019). MD 2, MD 3, and MD 4 exhibited considerably lower values than the original sample (MD 1), indicating that these models require less time to separate from the teeth/palate and are capable of forming a swallowable bolus (Figure 5). Conversely, MD 1 would make swallowing more challenging due to the formation of a denser network structure resulting from the aggregation of double helices during the steaming process (Liu, Chan et al., 2015).

As previously reported, dysphagia diets should have low hardness, appropriate adhesiveness, and requires little chewing effort (Suebsaen, Suksatit et al. 2019). Moreover, for 3D printing to be more desirable for elderly or dysphagia diets, the samples must possess sufficient mechanical strength to be self-supporting. Taking this into consideration, modifying the structure of the 3D printed surimi gel with a 2 mm hole size presents a feasible approach to developing 3D printed surimi gel that does not hinder the swallowing process. Therefore, based on its structural integrity, model MD 2 emerges as the most favorable gel sample with appropriate texture properties for the elderly or individuals with dysphagia.

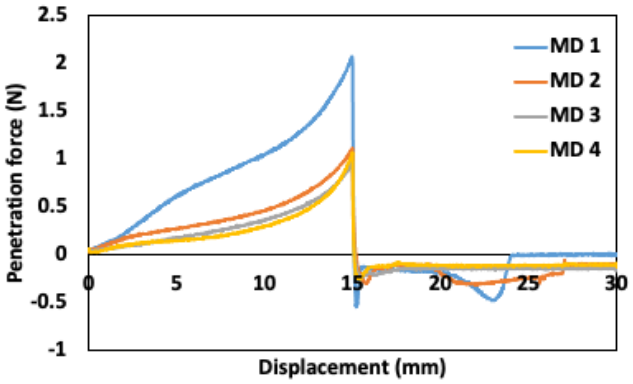


**Figure 5.** Texture properties of 3D printed surimi gel.

### 3.3. Evaluation of stress and strain properties of 3D printed surimi gel by numerical simulation

Table 1 and Figure 6 show the material properties and Johnson-Cook parameters used to simulate penetration of the 3D printed gel sample by cylindrical probe. The data fit was obtained using the ANSYS software.

**Table 1.** Surimi gel properties and Johnson-Cook parameters

| Parameter | Value |
|---|---|
| Young modulus, E (MPa) | 0.017 |
| Poisson's ratio | 0.4 |
| Density, ρ (kg/m$^{-3}$) | 0.97 |
| Initial yield strength, A (MPa) | 0.008 |
| Hardening modulus, B (MPa) | 0.012 |
| Strain hardening exponent, n | 0.675 |
| Strain rate constant, C | 0.07 |
| Reference strain rate, $\varepsilon_0$ (1/s) | 1 |

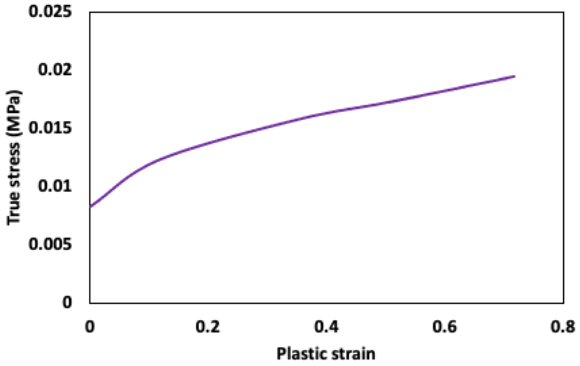


**Figure 6.** Curve of 3D printed surimi gel true stress vs plastic strain.

### 3.4. Numerical penetration test analysis on 3D printed gel

The stress curve resulting from the penetration analysis of 3D printed surimi gel is displayed in Figure 7. The von Mises criterion was employed to estimate the total contact stress, which encompasses the sum of shear and normal stress components within the gel sample (Triki and Gauvin, 2019). The simulation model successfully discerned variations in the true failure stress experienced by the gel samples at different failure distances (probe displacement), thereby allowing for a comprehensive characterization of the model design's influence on penetration characteristics. As illustrated in Figures 7a, stress dispersion occurred upon initial contact between the probe tip and the gel sample, generating an area of increasing stress as the probe penetrated the gel's surface. The impact of the model designs exhibited a significant difference between 0 and 6 mm displacements, with models MD 2, MD 3, and MD 4 displaying notably higher stress values compared to model MD 1. Stress in a material subjected to penetration force is calculated as the force (N) divided by the contact area (Triki and Gauvin, 2019). Due to the lower volume fraction in models MD 2, MD 3, and MD 4 compared to model MD 1, the density of the gel sample in contact with the penetrating probe is reduced. Additionally, the spaces between gel layers create regions that can be easily filled by the compressing sample, leading to the observed higher stress values at the initial stages of analysis. However, as compression and puncture progress, the gel sample becomes fully compacted (at a displacement of 6.28 mm), resulting in similar penetrative stress at this stage.

In general, for displacements greater than 6.28 mm (stress = 0.011 MPa), the stress value exhibited a steady increase for all samples until a displacement of 15 mm, which marked the end of the penetration. As the probe returned to its original position, the adhesive properties of the gel became evident, resulting in a bell-shaped curve at the peak of the stress-displacement relationship. After a few upward displacements by the probe, the stress value reached a constant level, indicating a decrease in the adhesive characteristics of the gel sample to the probe wall (Figure 7a).

Figure 8 illustrates the true strain-displacement curve of the 3D printed surimi gel. The strain property reflects the extent of deformation experienced by the gel sample under applied stress. It is determined by calculating the ratio of the change in length of the gel sample to its original length. When examined in relation to the applied force, it can be used to characterize the texture properties of food intended for the elderly or individuals with dysphagia, as it describes the level of deformation achieved at specific force values. In this study, a consistent force value of 0.05 N was applied to all samples, which corresponded to the trigger force used during the texture analysis. As observed in Figure 8a, the instantaneous strain values were significantly higher in models MD 4, MD 3, and MD 2 compared to MD 1 until a displacement of 6 mm. This suggests that MD 4 to MD 2 are more suitable for the elderly and individuals with dysphagia, as these samples exhibited greater deformation under the applied force.

Additionally, the maximum penetrative force of the 3D printed surimi gel was determined through numerical analysis (Figure 9). The penetrative force values exhibited a significant difference, with variations of approximately 50% between model MD 1 and the modified models (MD 2 to MD 4). This substantial decrease in penetrative force further confirms that gels of model MD 2 to MD 4 will require less chewing force.

Among the modified models, the penetrative force, stress, and strain characteristics are nearly similar. Considering that the integrity of the model's shape is also a critical factor in the development of 3D printed food, model MD 2 is recommended as the optimal design for developing 3D printed surimi gel for the elderly or individuals with dysphagia. This recommendation is based on the fact that as the volume of the sample decreases due to the creation of voids between the layers, the self-supporting ability of the 3D printed gel diminishes. Additionally, if the surface area of the paste is extensive, there will be more shrinkage and moisture loss during the steaming process.

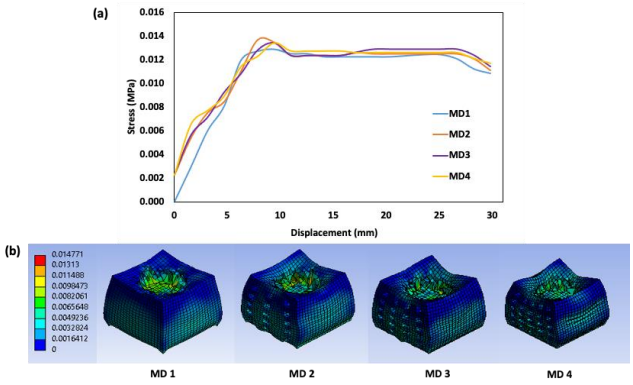


**Figure 7.** Stress-displacement curve of 3D printed surimi gel; (a) quantitative stress value and (b) contour description of the stress distribution in a puncture gel at a depth of 15 mm.

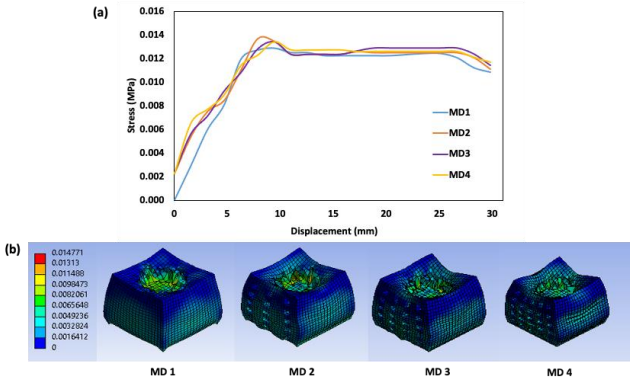


**Figure 8.** Strain-displacement curve of 3D printed surimi gel; (a) quantitative strain value and (b) contour description of the strain distribution in a puncture gel at a depth of 15 mm.

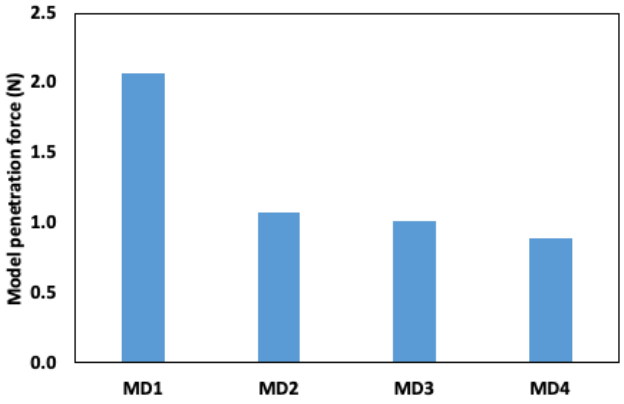


**Figure 9.** Simulated penetration for 3D printed surimi gel.

## 4. Conclusions

This study aimed to analyze the modification of texture characteristics in 3D printed surimi gel. The critical layer height for modifying the original sample (MD 1) was determined to be 2 mm. Based on this critical layer height, three models were developed with varying volume fractions (MD 2, MD 3, and MD 4). The stress and strain distribution of the samples during penetrative tests with a cylindrical probe were assessed using numerical simulation, specifically employing the Johnson-Cook model. The instantaneous penetration force of the 3D printed surimi gel highlighted the influence of the modified model's volume fraction, resulting in approximately a 50% decrease in penetrative force compared to the control (MD 1). Notably, models MD 2 to MD 4 exhibited high strain properties, indicating ease of deformability in the sample, making them suitable for seniors or individuals with dysphagia. The modified models displayed similar penetrative force, stress, and strain characteristics. Considering the significance of model shape integrity in the development of 3D printed food, model MD 2 is recommended as the optimal design for 3D printed surimi gel intended for seniors or individuals with dysphagia. This is attributed to the decreased self-supporting ability of the 3D printed gel as the volume fraction of the sample decreases. Moreover, the simulation results, particularly in penetrative force, align with the experimental findings, affirming the effectiveness of numerical analysis as a valuable method for developing suitable 3D printed food for specific consumer groups.

## Acknowledgements

This research was supported by the Basic Science Research Program through the National Research Foundation of Korea (NRF) funded by the Ministry of Education [grant number NRF-2018R1D1A3B06042501].

## References

Bhashyam, G. R. (2002). ANSYS mechanical—a powerful nonlinear simulation tool. Ansys, Inc, 1(1), 39.

Cao, H., Fan, D., Jiao, X., Huang, J., Zhao, J., Yan, B., ... & Zhang, H. (2018). Heating surimi products using microwave combined with steam methods: Study on energy saving and quality. Innovative Food Science & Emerging Technologies, 47, 231-240.

Duangmal, K., & Taluengphol, A. (2010). Effect of protein additives, sodium ascorbate, and microbial transglutaminase on the texture and colour of red tilapia surimi gel. International journal of food science & technology, 45(1), 48-55.

Hong, Y. K., Uhm, J. T., & Yoon, W. B. (2014). Using numerical analysis to develop and evaluate the method of high temperature Sous-Vide to soften carrot texture in different-sized packages. Journal of food science, 79(4), E546-E561.

Hsu, C. K., & Chiang, B. H. (2002). Effects of water, oil, starch, calcium carbonate and titanium dioxide on the colour and texture of threadfin and hairtail surimi gels. International journal of food science & technology, 37(4), 387-393.

Krasauskas, P., Kilikevičius, S., Česnavičius, R., & Pačenga, D. (2014). Experimental analysis and numerical simulation of the stainless AISI 304 steel

friction drilling process. Mechanika, 20(6), 590-595.

Lanier, T. C., Carvajal, P., & Yongsawatdigul, J. (2005). Surimi gelation chemistry. Surimi and surimi seafood, 2, 436-489.

Liu, S., Chan, W. L., & Li, L. (2015). Rheological properties and scaling laws of κ-carrageenan in aqueous solution. Macromolecules, 48(20), 7649-7657.

Medina, J. R., & Garrote, R. L. (2002). The effect of two cryoprotectant mixtures on frozen surubí surimi. Brazilian Journal of Chemical Engineering, 19, 419-424.

Oyinloye, T. M., & Yoon, W. B. (2022). Investigation of flow field, die swelling, and residual stress in 3D printing of surimi paste using the finite element method. Innovative Food Science & Emerging Technologies, 78, 103008.

Park, H. W., & Yoon, W. B. (2015). Measuring ring tensile stress and strain of surimi gels using a novel ring tensile test with image analysis. Journal of Food Engineering, 163, 9-16.

Song, B., & Sanborn, B. (2018). Relationship of compressive stress-strain response of engineering materials obtained at constant engineering and true strain rates. International Journal of Impact Engineering, 119, 40-44.

Suebsaen, K., Suksatit, B., Kanha, N., & Laokuldilok, T. (2019). Instrumental characterization of banana dessert gels for the elderly with dysphagia. Food Bioscience, 32, 100477.

Tabilo-Munizaga, G., & Barbosa-Cánovas, G. V. (2004). Color and textural parameters of pressurized and heat-treated surimi gels as affected by potato starch and egg white. Food research international, 37(8), 767-775.

Triki, E., & Gauvin, C. (2019). Analytical and experimental investigation of puncture-cut resistance of soft membranes. Mechanics of Soft Materials, 1, 1-11.

Wang, L., Zhang, M., Bhandari, B., & Yang, C. (2018). Investigation on fish surimi gel as promising food material for 3D printing. Journal of Food Engineering, 220, 101-108.

Zhang, X., Chu, X., Ji, H., & Wang, Y. (2016). Effect of freezing rate on the onion cell deformation evaluated by digital image correlation. Food Analytical Methods, 9, 3125-3132.